Journal of Materials Science: Materials in Electronics (2019) 30:19060–19068
https://doi.org/10.1007/s10854-019-02263-3

Determination of some properties of ZnSB thin films deposited by a thermionic vacuum arc technique

Sedat Sürdem[1]

Received: 20 June 2019 / Accepted: 23 September 2019 / Published online: 26 September 2019

Abstract

In this work, thin films of ZnSB were deposited by a thermionic vacuum arc technique. ZnSB thin films were deposited to various substrates such as glass, polyethylene terephthalate and silicon wafer. Structural, optical, morphological properties and chemical analysis of ZnSB thin films were investigated. The thicknesses values of the thin films were measured as to be 60 nm, 5 nm and 40 nm on glass, PET and Si substrates, respectively by using interferometer. The X-ray diffraction (XRD) were used to identify the structural characteristics of the thin films. ZnSB thin films were observed in polycrystalline structures from the XRD results. UV–Visible spectrophotometer were carried out to determine optical properties of ZnSB thin films. The average transmittance values of the ZnSB thin films were obtained to be 89% and 85% on glass and PET substrates, respectively. The band gap energy for ZnSB thin films were estimated as 3.69 eV and 3.54 eV on glass and PET substrates. By using photoluminescence spectroscopy, ZnSB thin films are located at 413 nm (3.08 eV) where is known as near band emission band. From FESEM and AFM analyses, ZnSB thin films have exhibited smoothness, uniform and densely formed surface profile. Chemical analyses of ZnSB thin films were carried out by Raman spectroscopy. Considering Raman spectra of ZnSB thin films, ZnS peaks were observed mainly.

1 Introduction

Zinc sulfide (ZnS) is one of the most important stable II–VI semiconductor material [1]. ZnS exhibits n-type conductivity, high transparency (> 94%), very high resistivity, large exciton-binding energy (~ 40 meV) and has direct wide band gap (3.2–3.9 eV) at room temperature. ZnS consists of two crystal structures as a cubic phase (zinc blend) and a hexagonal phase (wurtzite). On the other hand, ZnS is a low-priced and abundant raw material. In addition, it is chemically and mechanically stable and non-toxic [1–7]. ZnS thin film is a promising material for Cu(In,Ga)Se_2 (CIGS) based solar cells [1], window layer material solar cells, ultra-violet (UV) light emitting diodes (LEDs) [8], flat panel displays, field effect transistors (FET), infrared (IR) windows [9], optical sensors [10], lasers, reflectors [1, 4, 5, 11]. According to the literature, ZnS thin films could be deposited with different techniques such as ion beam sputtering [12], radio-frequency (RF) sputtering [13], chemical vapor deposition (CVD) [14], electrochemical deposition [15], spray pyrolysis [16], chemical bath deposition (CBD) [17], sol–gel [18], thermal evaporation [19] and electron beam (e-beam) evaporation [20] on various type of substrates. As it is known, when appropriate dope material is chosen, structural, optical and electrical properties of the ZnS thin films might in significant changes as well. According toliterature, various elements such as Cu, Ag, Al, Ga, Ti, Cd, Cr and B have been doped to ZnS [21–28]. Among group III elements, Boron (B) has an attractive material due to unique properties and wide applications. Also, Boron is close to the refractory metals and very suitable candidate for p-type doping in semiconductors. Nevertheless, boron doped ZnS thin films seem less discussed when the literature has been reviewed.

In this study, the ZnSB thin films were prepared on amorphous glass, semi crystalline polyethylene (PET) and silicon (Si) substrates by TVA technique. The structural, optical, surface properties and chemical analysis of ZnSB thin films were reported. X-ray diffractometer (XRD) were utilized to determine the structural and phase properties of the prepared ZnSB thin films. The optical properties of ZnSB thin films were investigated by using interferometer, UV–Vis and photoluminescence (PL) spectroscopic techniques. Surface properties of the ZnSB thin films were analyzed by Field

✉ Sedat Sürdem
sedat@boren.gov.tr

[1] National Boron Research Institute, 06520 Ankara, Turkey

Emission Scanning Electron Microscopy (FESEM) and Atomic Force Microscopy (AFM). Raman spectroscopy measurements were applied for obtaining chemical information about ZnSB thin films.

Thermionic vacuum arc (TVA) technique is a fast, low-cost and eco-friendly nanocrystalline thin film deposition technique in high vacuum conditions. By means of TVA technique, thin films can be deposited at room temperature upon substrates which have even low melting points. This technique does not require heating the substrates during thin film deposition. Also, no buffer gas is needed and no sophisticated instrumentation is required in this technique. Thin films deposited by TVA technique have a number of advantage like homogeneity, compactness, good adhesion, low roughness, high deposition rate and short processing time.

2 Experimental

TVA is a thin film growth technique and unique method to produce nanostructured thin films. In this technique, high-temperature annealing is no necessary. So far, there have been various reported studies in the literature about TVA technique [29–37]. TVA is a rapid plasma assisted thin film deposition technology. TVA is based on the anodic pure plasma generation. TVA system has two main components as anode and cathode electrodes. The anode consists of spoon like crucible oftungsten or molybdenum andan evaporation material. The cathode is an electron gun including tungsten filament with a diameter of 0.5 mm which is mounted inside an electron-focusing a Wehnelt cylinder. The distance is 5–6 mm between the electrodes. In this study, the boron (B) piece (Alfa Aesar, 99.95%) and zinc sulfide (ZnS) granule (Don Co., Ltd.) were used as anode material and ZnSB thin films were deposited on amorphous glass microscope slide, semi-crystalline polyethylene terephthalate (PET) and silicon (Si) wafer substrates. B piece and ZnS granule were placed into tungsten evaporation crucible. Unlike other vacuum techniques, anode materials like granule, pellet, pieces, rod, etc. can be placed into crucible in this technique. ZnS and B materials were used as co-evaporation sources. Plasma of ZnS and B anode materials was created using an electron beam simultaneously. So, the possibility of co-processing of ZnS and B mixure were presented. The vacuum chamber was pumped down to base pressure (6×10^{-5} torr). In the deposition process, thermionic electrons were emitted from the tungsten filament and then the electrons were focused onto evaporation material (ZnSB) by aWehnelt cylinder. High voltage potential is being forced to heat and evaporates ZnSB materials. Thus, ZnSB materials start to be deposited on the glass, PET and Si substrates. The TVA discharge occurs between the anode and cathode electrodes under high vacuum conditions. During deposition of ZnSB thin films, vacuum chamber pressure was 1.18×10^{-4} torr. Filament current and voltage applied to cathode was 21.2 A and 18.5 V, respectively. However, voltage between anode and cathode was 200 V in the space and created discharge current between anode and cathode was 0.05 A. The deposition process duration was just 5 min at room temperature. Schematic view of the TVA system is seen in Fig. 1.

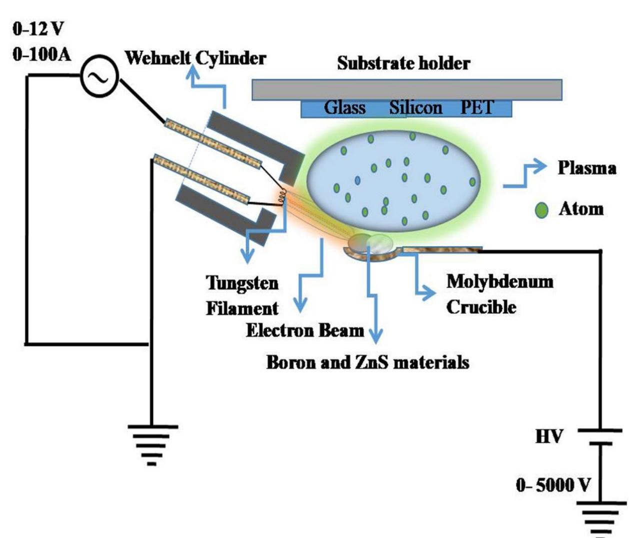

Fig. 1 Schematic view of the TVA system for ZnSB deposition

3 Results and discussion

Choice of deposition techniques and substrate materials are playing an important role in the microstructural properties. Generally, polycrystalline films can not be deposited on glass substrate at low temperatures. Whereas, it is possible with TVA technique having higher ion energy. At the same time, nature of substrates are important as well.

The crystal structure and phase properties of the ZnSB thin films were studied using (PANalytical/Empyrean) X-ray diffractometer (XRD). XRD patterns were obtained in the 2θ range of 20°–70° with Cu-Kα radiation source ($\lambda = 0.154$ nm) for the pristine ZnS and ZnSB thin films. The XRD patterns of ZnS and ZnSB thin films are displayed in Fig. 2. All the diffraction peaks in pristine ZnS belong to hexagonal and cubic phases of ZnS. The diffraction peaks at 26.94°, 27.88°, 28.54°, 30.50°, 33.10°, 39.62°, 45.56°, 47.52°, 51.86°, 56.39° and 57.66° correspond to the (100), (101), (111), (101), (020), (012), (015), (202), (016), (111) and (201) planes, respectively. As can be seen in Fig. 2, ZnS, Zn, B, B_8S_{16} and S_5Zn_5 reflections were detected at various degrees. It was concluded that while polycrystalline ZnSB thin films were deposited on glass and PET substrates, single

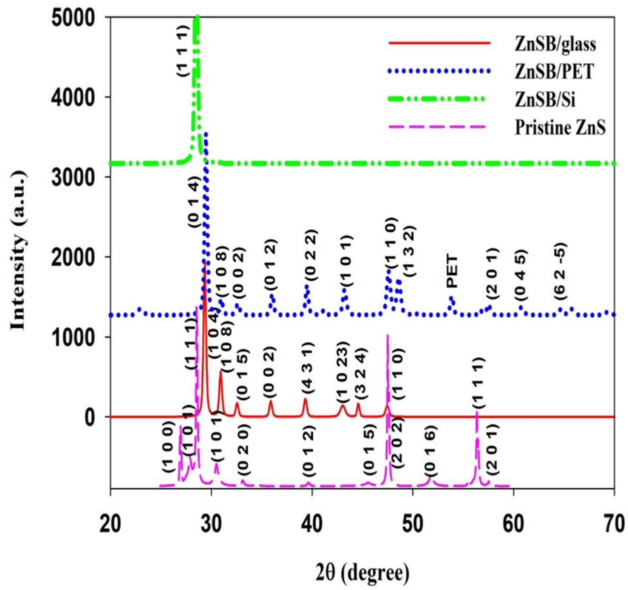

Fig. 2 XRD patterns of the ZnSB thin films deposited on the glass, PET and Si substrates

crystalline ZnSB thin film was deposited on Si substrate. As the XRD patterns compared, it can be seen that microstructure properties and intensities of the peaks are quitely different. Microstructure properties of ZnSB thin films were affected due to different structure of substrate materials which are amorphous glass, semi-crystalline PET and Si wafer. The peaks of ZnS and B were observed at different 2θ values on glass and PET substrates. In this situation, it caused a shift of 2θ values due to background effect of glass and PET substrates. Peak positions, miller indices and crystal structures along with their reference Crystallography Open Database ID (COD ID) numbers were given in Table 1. These results are in harmony with the literature [38–45].

The refractive index (n) versus wavelength (λ) and thicknesses were measured simultaneously by using Filmetrics F20 tool. ZnSB thin film layers were measured as approximately 60 nm, 5 nm and 40 nm on glass (ZnSB/glass), on PET (ZnSB/PET) and on Si (ZnSB/Si) substrates, respectively. The differences in the thicknesses are due to the distance differences between anode and substrates (see Fig. 1). ZnS/PET thin film thickness was found to be less because the PET substrate was placed further away from the glass and Si substrates. In the refractive index measurements, Cauchy dispersive model is used where the films are transparent. It is well known that the refractive index (n) varies as a function of wavelength. That is, produced thin films exhibit the normal dispersion behavior in the visible wavelength range. The graph of refractive index and reflectance is shown in Fig. 3a. Refractive indices of ZnSB/glass and ZnS/PET thin films were measured as 1.54 and 2.21 at 550 nm, respectively. According to Fig. 3a refractive index values of ZnSB/glass and ZnSB/PET thin films are decreased with increased wavelength. This case related to both different of density and compactness of deposited layers and difference

Table 1 Determined XRD parameters of ZnSB thin films on glass, PET and Si substrates

	2θ (°)	Diffraction plane	Miller indices	Crystal system	COD ID
ZnSB/glass	29.36	S_5Zn_5	(1 0 4)	Hexagonal	9000085
	30.92	S_5Zn_5	(1 0 8)	Trigonal (hexagonal axes)	9013410
	32.58	ZnS	(0 1 5)	Hexagonal	9000086
	35.89	Zn	(0 0 2)	Hexagonal	1512553
	39.29	B	(4 3 1)	Trigonal (rhombohedral axes)	9011109
	43.07	ZnS	(1 0 23)	Trigonal (hexagonal axes)	2310815
	44.54	B	(3 2 4)	Trigonal (hexagonal axes)	9012122
	47.48	ZnS	(1 1 0)	Hexagonal	100044
ZnSB/PET	29.45	S_5Zn_5	(1 0 4)	Hexagonal	9000085
	30.92	S_5Zn_5	(1 0 8)	Trigonal (hexagonal axes)	9013410
	32.67	ZnS	(1 0 31)	Trigonal (hexagonal axes)	2310813
	36.07	Zn	(0 0 2)	Hexagonal	9011599
	39.48	ZnS	(0 1 2)	Hexagonal	1011196
	41.13	B	(0 2 2)	Tetragonal	9012309
	43.25	Zn	(1 0 1)	Hexagonal	9011599
	47.57	ZnS	(1 1 0)	Trigonal (hexagonal axes)	2310814
	48.59	B	(1 3 2)	Tetragonal	9012310
	57.51	ZnS	(2 0 1)	Hexagonal	1101051
	60.82	S	(0 4 5)	Orthorhombic	9012334
	65.79	$B_8 S_{16}$	(6 2 – 5)	Monoclinic	1511701
ZnSB/Si	28.53	ZnS	(1 1 1)	Cubic	1538617

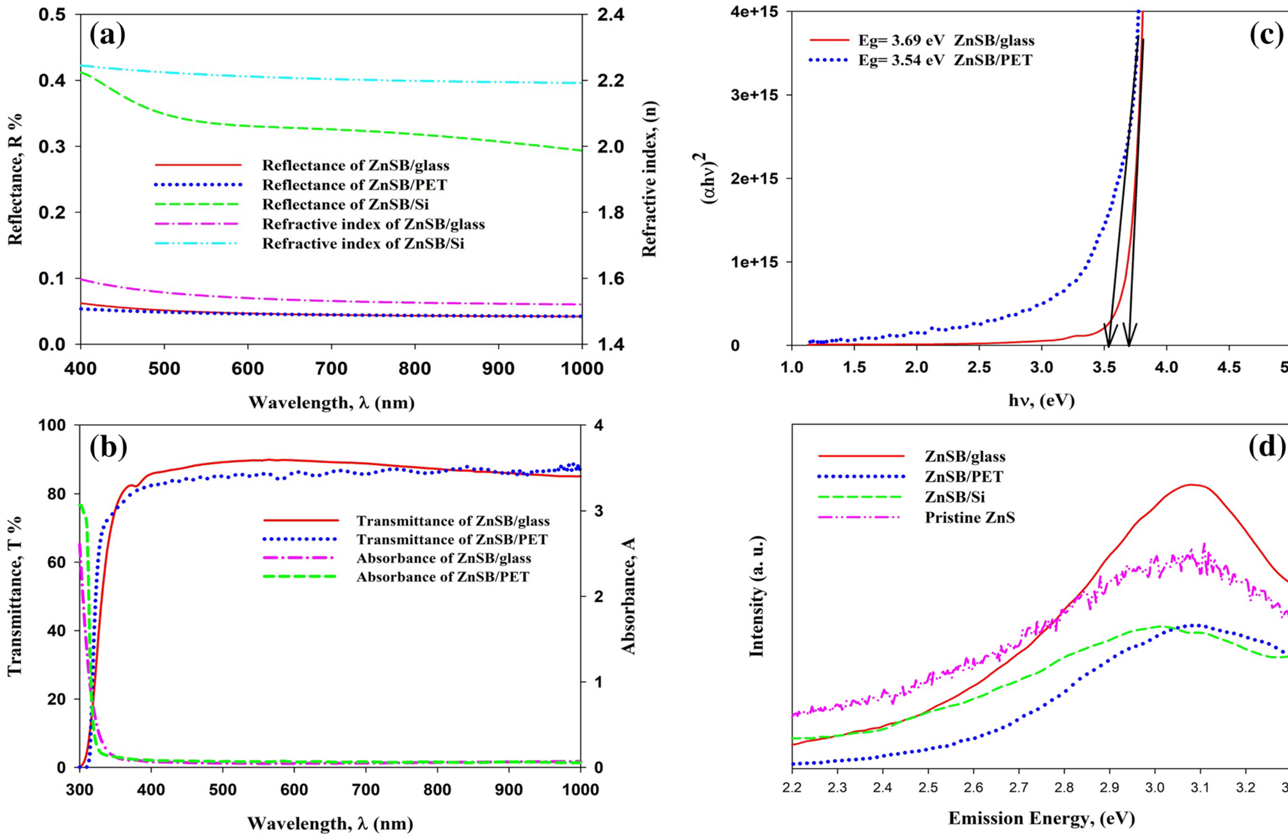

Fig. 3 Optical properties of ZnSB thin films **a** reflectance and refractive index, **b** transmittance and absorbance, **c** band gap and **d** PL spectra graphs

of crystal structure because of substrate effect. Obtained refractive indices of ZnSB thin films are in good agreement with literature [1, 3, 4, 11].

Optical reflectance of ZnSB thin films were measured simultaneously with Filmetrics F20 tool and illustrated in Fig. 3a. As displayed in the figure, the intensity of optical reflectance were approximately 4% over the visible spectral region for ZnSB/glass and ZnSB/PET thin films. This situation indicated that the reflectance values of ZnSB/glass and ZnSB/PET thin films were almost the same where produced thin films were transparent. Reflectance values decreases because of defects, grain boundaries, smaller grains and crystalline imperfections [5]. Meantime, optical reflectance for ZnSB/Si thin film is 33% at 550 nm which is higher than the others. This observation can be related to the effect of substrates. Therefore, the reflectance spectra is in harmony with the XRD results.

The optical transmittance and absorbance of the ZnSB thin films were recorded by an Unico UV–Vis spectrophotometer in the wavelength range of 300–1100 nm. As it is known, grain boundaries of thin films absorb the visible light and exhibit high absorbing properties. The transmittance and absorbance graph of the ZnSB thin films were presented in the same Fig. 3b for comparison. ZnSB/glass and ZnSB/PET thin films were behaved as transparent in the visible region. Transmittance values of ZnSB/glass and ZnSB/PET thin films at 550 nm were measured as 89% and 85%, respectively. In this stiation, ZnSB/glass and ZnSB/PET thin films indicate that they are optically similar [37]. However, crystallinity of the films can lead to higher transparency. It is note worthy that ZnSB thin films exhibit low absorption in the infrared region. A steep absorption edge at ~ 310 nm was observed in the fundamental absorption region. The steep absorption in this region can be associated with homogeneous grain distribution.

Band gap of thin films is an important optical parameter. Tauc formula which is well – known and a simple methodis used to determine the band gap energy [46]:

$$\alpha h\nu = A(h\nu - E_g)^n \quad (1)$$

where A is a constant, $h\nu$ is incident photon energy, α is the absorption coefficient and, E_g is represented as band gap energy of the thin films in the formula. In addition, n value indicates the electronic transitions of materials and can get four different values (1/2, 2, 3/2 or 3). These values are related with direct and indirect forbidden transitions. As can be seen from Fig. 3c, optical band gap energy E_g were estimated by drawing the Tauc plot of $(\alpha h\nu)^2$ versus $h\nu$. The optical absorption coefficient α, can be calculated using the following relation:

$$\alpha = \frac{1}{d}\ln(1/T) \tag{2}$$

where, d and T are the thickness and transmittance values for the thin films, respectively. As can be noticed, the band gap energy of ZnSB/glass and ZnSB/PET thin films were obtained as 3.69 eV and 3.54 eV respectively, which is in agreement with previous studies [2–4, 36, 37, 47]. However, band gap structure of ZnSB/glass thin film, is sharp and smooth. That is defect level is lower than ZnSB/PET thin film.

Photoluminescence (PL) spectroscopy is an appropriate technique for investigation of crystalline quality, defects of the deposited films and band gap energy E_g of different materials. The PL spectra were obtained over the wavelength range 350–520 nm with 330 nm excitation for the ZnSB thin films by using Perkin-Elmer LS-55 device at room temperature. Figure 3d displays PL spectra for the comparison of pristine ZnS material and all ZnSB thin films. Pristine ZnS material peak is located at 400 nm (3.10 eV). This PL emission peak is known as near band emission (NBE) band. On the other hand, ZnSB thin films are located at 413 nm (3.08 eV). However, these emission peaks are related to crystalline defects, impurity levels, defect levels, vacancies and interstitials. In our study, we concluded that the NBE peak of ZnS is shifted from 400 nm to 413 nm with the effect of B in thin films. The emissions at 3.08 eV stand for a transition from the conduction band to the I_S level. These values are very good harmony with literature [3, 5, 37, 48].

Raman spectroscopy, which is sensetive and non-destructive method, gives information on materials. Raman analyses of ZnSB thin films were performed on a Renishaw inVia spectrometer using 532 nm laser (2.33 eV) excitation source. Raman spectra of the pristine ZnS material and ZnSB thin films are seen in Fig. 4. Position of pristine ZnS peaks were found at 178, 216, 272, 348 (strong), 672 cm^{-1}, respectively. Observed peaks were characteristic raman peaks of ZnS. As can be seen, Raman shifts detected was related with ZnS. Raman shift peaks of PET and silicon substrates were also detected. According to earlier studies reported that Raman shift center at around 350 cm^{-1} the longitudinal optical (LO) Raman mode in the cubic and hexagonal phases of ZnS [49]. ZnS peak was detected at around 355 cm^{-1} for ZnSB/glass thin film [50]. For ZnSB/PET thin film, the position of ZnS peaks were detected at 112, 153, 223, 282, 380 and 1095 cm^{-1} respectively [7, 39, 50]. It was observed that the characteristic ZnS Raman peaks shifts to due to boron effect. Other peaks observed were from background of PET substrate. In the same way, ZnSB/Si thin film shows ZnS

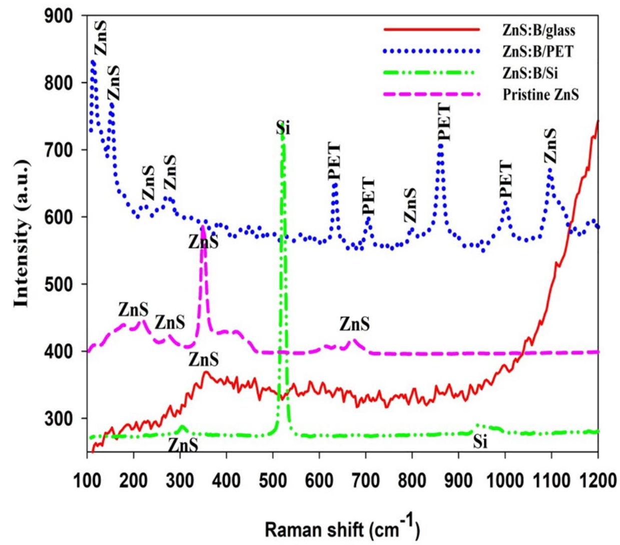

Fig. 4 Raman spectra of ZnSB thin films

peak which lies at around 303 cm^{-1} [39, 51]. The peaks were observed at 520 and 942 cm^{-1} from the silicon substrate. Besides, we could not observe raman peaks of B in the spectrum. This suggests that the smaller radius and low amount of boron does not change the vibrational modes of ZnS, significantly.

The surface properties of the ZnSB thin films were investigated with both field emission scanning electron microscopy (FESEM) and atomic force microscopy (AFM). Carl Zeiss Supra 55 model was used for high-resolution surface imaging analyses. The FESEM images of ZnSB thin films with a magnification of 300 kx can be seen from Fig. 5a–c. It can be observed that ZnSB thin films exhibit dense, homogeneous and almost similar to each other from Fig. 6a–c. Although under the same conditions deposited ZnSB/glass and ZnSB/Si thin films exhibited smoth and uniform distributions, ZnSB/PET thin film was appeared with presence of cracks. The formation of this cracks may be due to thermal expansion of the PET surface.

Average roughness (Ra) measurements and height distribution graph of the ZnSB thin films were used AFM (Ambios Q-scope atomic force microscope) device to obtain 2D and 3D surface imaging. All measurements were done in non-contact mode using the Scan Atomic V 5.1.0 SPM control software at room temperature. The 2D and 3D AFM images of ZnSB thin films were scanned in the range of 2×2 μm^2 and shown in Fig. 6a–f. Also, the height distribution graph is plotted in Fig. 6g. As can be seen that images of ZnSB thin films are very similar to each other, nano-structured and having very smooth surface. Average roughness (Ra) is the mean value of the surface height with respect to a center plane [52]. Using 7 lines measurement at this scale, Ra values were approximately 0.53 nm, 0.76 nm

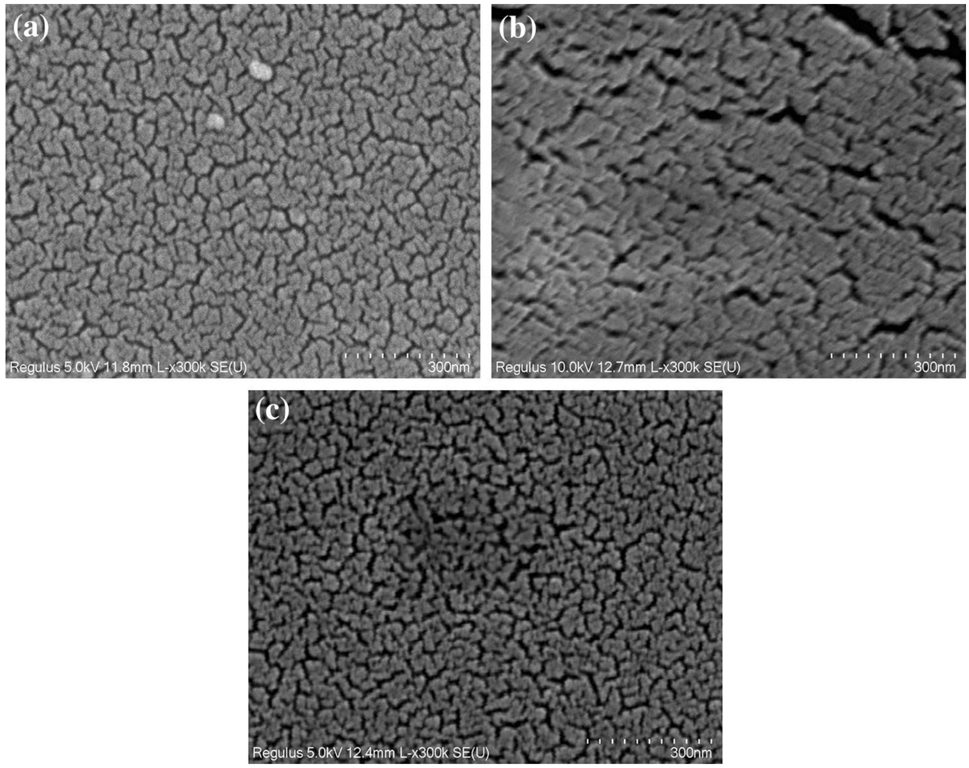

Fig. 5 FESEM images of ZnSB thin films deposited on glass (**a**), PET (**b**) and Si (**c**) substrates

and 0.46 nm for ZnSB/glass, ZnSB/PET and ZnSB/Si, respectively. These low values confirm the smooth surface of ZnSB thin films. It means that, this Ra values of ZnSB/glass and ZnSB/Si thin films were smoother than Ra value of ZnSB/PET. Because the lattice mismatch had not appeared between ZnSB/glass and ZnSB/Si thin films and substrates.

FESEM images of ZnSB thin films support AFM images. In addition, the height distribution histogram of ZnSB thin films is shown in Fig. 6g. According to the height distribution histogram analysis of ZnSB thin films exhibited homogeneous grain distribution over the surfaces. This situation can be explain related to Gauss curve. It is evident that in the ZnSB/Si thin film was determined better Gauss curve than the others due to low roughness of ZnSB/Si thin film.

4 Conclusion

In conclusion, ZnSB thin films were produced on glass, PET and Silicon substrates using TVA technique and were characterized by XRD, optical, morphological and chemical measurements. The XRD patterns of ZnSB showed that produced thin films have an polycrystalline character. The produced ZnSB thin films were determined to be wide band gap semiconductors. Also, band gap of ZnSB/glass and ZnSB/PET thin films were calculated as 3.69 eV and 3.54 eV, respectively. Transmittance spectrum of ZnSB thin films have demonstrated high optical transmittance 85–89% at 550 nm. ZnSB/glass and ZnSB/PET thin films have lower reflection 4% while maximum reflection for ZnSB/Si thin film exhibits about 33%. In this situation, a higher level of reflectance can be understood due to the Si substrate. Refractive index values of ZnSB thin films were good agreement with literature. Raman spectroscopy measurements were applied. Raman spectrum related with ZnS and ZnSB were detected. It was observed that the amount of boron does not significantly change the vibrational modes of ZnS. Meantime, morphological properties of ZnSB thin films were reported. FESEM and AFM images showed that all ZnSB thin films were homogeneous and uniformly distributed over the surface. Ra values of produced ZnSB thin films were determined 0.53 nm, 0.76 nm and 0.46 nm for glass, PET and Si substrates, respectively. However, a symmetrical Gaussian surface distribution were observed for ZnSB thin films. ZnSB thin films deposited on three different substrates exhibited almost the same properties.

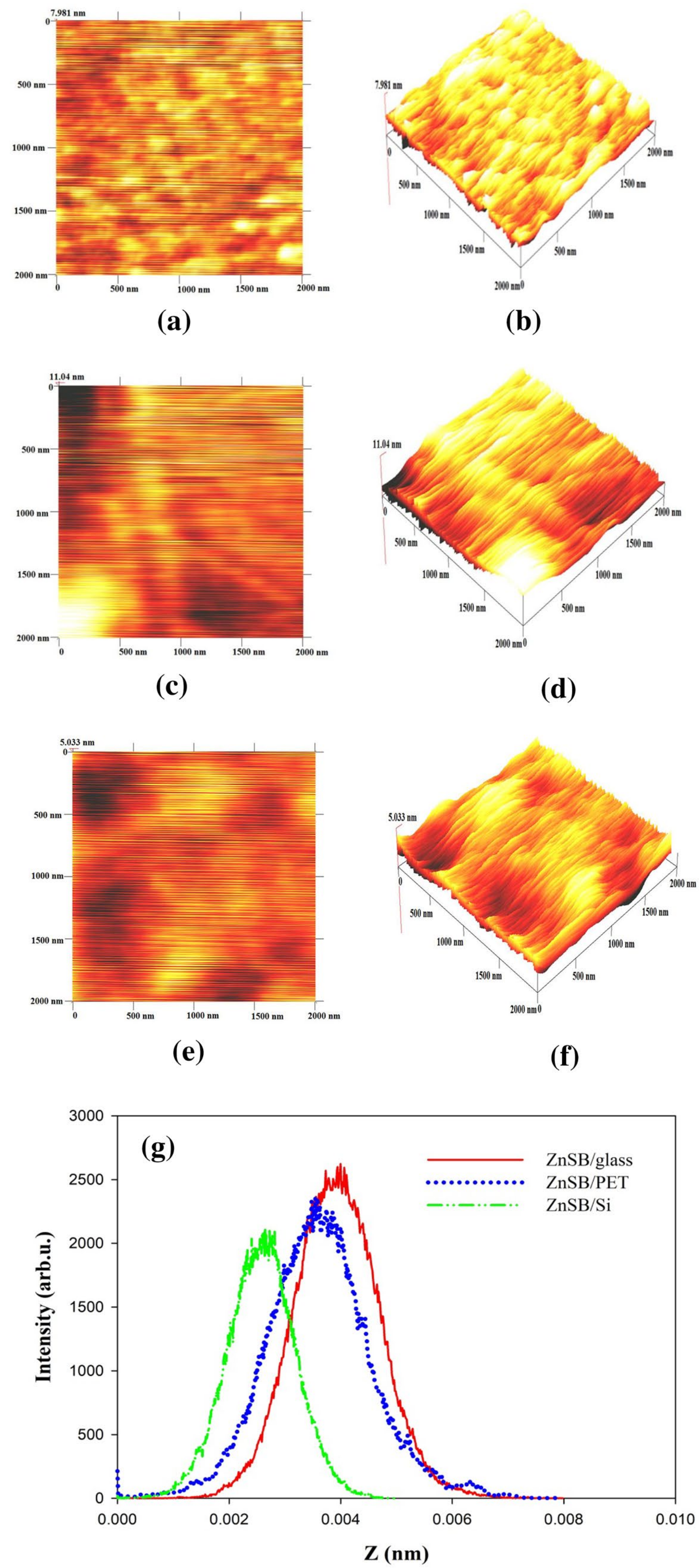

Fig. 6 2D and 3D AFM images of the **a**, **b** ZnSB/glass, **c**, **d** ZnSB/PET, **e**, **f** ZnSB/Si thin films and **g** height distribution graph of ZnSB thin films

Acknowledgements Author thanks to S. Elmas, N. Akkurt and R. Mohammadigharehbagh for thin film deposition and contributions.

References

1. S.M. Mosavi, H. Kafashan, Physical properties of Cd-doped ZnS thin films. Superlattices Microstruct. **126**, 139–149 (2019)
2. X. Yang, B. Chen, J. Chen, Y. Zhang, W. Liu, Y. Sun, ZnS thin film functionalized as back surface field in Si solar cells. Mater. Sci. Semicond. Process. **74**, 309–312 (2018)
3. A. Azmand, H. Kafashan, Al-doped ZnS thin films: physical and electrochemical characterizations. J. Alloys Compd. **779**, 301–313 (2019)
4. F. Zakerian, H. Kafashan, Investigation the effect of annealing parameters on the physical properties of electrodeposited ZnS thin films. Superlattices Microstruct. **124**, 92–106 (2018)
5. A. Azmand, H. Kafashan, Physical and electrochemical properties of electrodeposited undoped and Se-doped ZnS thin films. Ceram. Int. **44**, 17124–17137 (2018)
6. S.L. Patel, A. Purohit, S. Chander, M.S. Dhaka, Thermal annealing evolution to physical properties of ZnS thin films as buffer layer for solar cell applications. Physica E **101**, 174–177 (2018)
7. T. Hurma, Studies of structural, optical and electrical properties of nanostructured ZnS: F films. Optik **174**, 324–331 (2018)
8. A. Jrad, W. Naffouti, T. Ben Nasr, N. Turki-Kamoun, Comprehensive optical studies on Ga-doped ZnS thin films synthesized by chemical bath deposition. J. Lumin. **173**, 135–140 (2016)
9. N.V. Nghia, N.D. Hung, Photoluminescence emission of Cu doped ZnS microstructures synthesized by thermal evaporation. VNU J. Sci. Math. Phys. **34**, 1–7 (2018)
10. M.E. Pacheco, C.B. Castells, L. Bruzzone, Mn-doped ZnS phosphorescent quantum dots: coumarins optical sensors. Sens. Actuators B **238**, 660–666 (2017)
11. N. Tajik, M.H. Ehsani, R. Zarei Moghadam, H. Rezagholipour Dizaji, Effect of GLAD technique on optical properties of ZnS multilayer antireflection coatings. Mater. Res. Bull. **100**, 265–274 (2018)
12. J. Kennedy, P.P. Murmu, P.S. Gupta, D.A. Carder, S.V. Chong, Effects of annealing on the structural and optical properties of zinc sulfide thin films deposited by ion beam sputtering. Mater. Sci. Semicond. Process. **26**, 561–566 (2014)
13. D.H. Hwang, J.H. Ahn, K.N. Hui, K.S. Hui, Y.G. Son, Structural and optical properties of ZnS thin films deposited by RF magnetron sputtering. Nanoscale Res. Lett. **7**, 26–32 (2012)
14. Q. Zhong, H. Kou, L. Yang, Y. Tao, C. Luo, Z. Xu, Factors influencing variations in the thermal conductivity of polycrystalline ZnS and Cr^{2+}:ZnS. Mater. Lett. **158**, 222–224 (2015)
15. K. Ghezali, L. Mentar, B. Boudine, A. Azizi, Electrochemical deposition of ZnS thin films and their structural, morphological and optical properties. J. Electroanal. Chem. **794**, 212–220 (2017)
16. K.B. Bacha, A. Timoumi, N. Bitri, H. Bouzouita, Structural, morphological and optical properties of sprayed ZnS thin films on various substrate natures. Optik **126**, 3020–3024 (2015)
17. F. Gode, C. Gumus, M. Zor, Investigations on the physical properties of the polycrystalline ZnS thin films deposited by the chemical bath deposition method. J. Cryst. Growth **299**, 136–141 (2007)
18. M.S. Akhtar, S. Riaz, S. Naseem, Optical properties of sol-gel deposited ZnS thin films: spectroscopic ellipsometry. Mater. Today Proc. **2**, 5497–5503 (2015)
19. R. Vishwakarma, Effect of substrate temperature on ZnS films prepared by thermal evaporation technique. J. Theor. Appl. Phys. **9**, 185–192 (2015)
20. X. Wu, F. Lai, Y. Lin, Z. Huang, R. Chen, Effects of substrate temperature and annealing on the structure and optical properties of ZnS film. Proc. SPIE **6722**(1–6), 67222 (2007)
21. S.R. Chalana, R.J. Bose, R.R. Krishnan, V.S. Kavitha, R. Sreeja Sreedharan, V.P.M. Pillai, Structural phase modification in Cu incorporated nanostructured zinc sulfide thin films. J. Phys. Chem. Solids **95**, 24–36 (2016)
22. E.G. Alvarez-Coronado, L.A. González, J.C. Rendón-Ángeles, M.A. Meléndez-Lira, R. Ramírez-Bon, Study of the structure and optical properties of Cu and Mn in situ doped ZnS films by chemical bath deposition. Mater. Sci. Semicond. Process. **81**, 68–74 (2018)
23. K. Yadav, N. Jaggi, Effect of Ag doping on structural and optical properties of ZnSe nanophosphors. Mater. Sci. Semicond. Process. **30**, 376–380 (2015)
24. D. Amaranatha Reddy, C. Liu, R.P. Vijayalakshmi, B.K. Reddy, Effect of Al doping on the structural, optical and photoluminescence properties of ZnS nanoparticles. J. Alloys Compd. **582**, 257–264 (2014)
25. H. Naz, R.N. Ali, X. Zhu, B. Xiang, Effect of Mo and Ti doping concentration on the structural and optical properties of ZnS nanoparticles. Physica E **100**, 1–6 (2018)
26. J. Kumar, R. Thangaraj, S. Sharma, R.C. Singh, Enhanced dielectric permittivity and photoluminescence in Cr doped ZnS nanoparticles. Appl. Surf. Sci. **416**, 296–301 (2017)
27. K. Lee, Y. Kim, N. Song, I.-H. Choi, S.Y. Park, Structural, optical, and electrical properties of boron-doped ZnO1-xSx thin films deposited by MOCVD. Curr. Appl. Phys. **19**, 14–19 (2019)
28. Ö.I. Ceviz, Y. Özdemir, M. Bedir, M. Öztaş, Effect of the substrate temperature on the characterization of spray-deposited ZnS: B films developed ın scıence parks. J. Optoelectron. Biomed. Mater. **5**, 51–55 (2013)
29. N. Ekem, T. Akan, S. Pat, M.Z. Balbag, M.I. Cenik, E. Karakas, R. Vladoiu, G. Musa, Investigation of properties of boron thin film deposited by thermionic vacuum arc technology. AIP Conf. Proc. **1**, 699 (2007)
30. M. Özgür, S. Pat, R. Mohammadigharehbagh, C. Musaoğlu, U. Demirkol, S. Elmas, S. Özen, Ş. Korkmaz, Sn doped ZnO thin film deposition using thermionic vacuum arc technique. J. Alloys Compd. **774**, 1017–1023 (2019)
31. M. Özgür, S. Pat, R. Mohammadigharehbagh, C. Musaoğlu, U. Demirkol, S. Elmas, S. Özen, Ş. Korkmaz, J. Mater. Sci.: Mater. Electron. **30**, 624–630 (2019)
32. S. Elmas, S. Pat, R. Mohammadigharehbagh, C. Musaoğlu, M. Özgür, U. Demirkol, S. Özen, Ş. Korkmaz, Determination of physical properties of graphene doped ZnO (ZnO: Gr) nanocomposite thin films deposited by a thermionic vacuum arc technique. Phys. B **557**, 27–33 (2019)
33. S. Pat, Ş. Korkmaz, S. Özen, V. Şenay, The effects of boron alloying on the structural and optical properties of GaAs deposited by a thermionic vacuum arc method. Mater. Focus **5**, 1–4 (2016)
34. S. Elmas, Ş. Korkmaz, S. Pat, Investigation of physical properties and surface free energy of produced ITO thin films by TVA technique. J. Mater. Sci.: Mater. Electron. **30**(9), 8876–8882 (2019)
35. S. Pat, S. Özen, Ş. Korkmaz, A rapid method for deposition of Sn-doped GaN thin films on glass and polyethylene terephthalate substrates. J. Electron. Mater. **47**, 167–172 (2018)
36. M. Ozkan, N. Ekem, S. Pat, M.Z. Balbağ, ZnS thin film deposition on silicon and glass substrates by thermionic vacuum Arc. Mater. Sci. Semicond. Process. **15**, 113–119 (2012)
37. H.K. Kaplan, S.K. Akay, M. Ahmetoglu, Photoelectrical properties of fabricated ZnS/Si heterojunction device using thermionic

vacuum arc method. Superlattices Microstruct. **120**, 402–409 (2018)
38. H.T. Evans, E.T. McKnight, New wurtzite polytypes from Joplin, Missouri. Am. Miner. **44**, 1210–1218 (1959)
39. S. Mardix, E. Alexander, O. Brafman, I.T. Steinberger, Polytype families in zinc sulfide crystals. Acta Crystallogr. **22**, 808–812 (1967)
40. K. Lejaeghere, V. Van Speybroeck, G. Van Oost, S. Cottenier, Error estimates for solid-state density-functional theory predictions: an overview by means of the ground-state elemental crystals. Crit. Rev. Solid State Mater. Sci. **39**, 1–24 (2014)
41. J.L. Hoard, D.B. Sullenger, C.H.L. Kennard, R.E. Hughes, The structure analysis of beta-rhombohedral boron. J. Solid State Chem. **1**, 268–277 (1970)
42. C. Frondel, C. Palache, Three new polymorphs of zinc sulfide. Science **107**, 602 (1948)
43. E.A. Jumpertz, Electron-density distribution in zinc blende. Z. Elektrochem. **59**, 419–425 (1955)
44. A.W. Hull, W.P. Davey, Graphical determination of hexagonal and tetragonal crystal structures from X-ray data. Phys. Rev. **17**, 549–570 (1921)
45. R. Juza, A. Rabenau, G. Pascher, Ueber feste Loesungen in den Systemen Zn S-Mn S, Zn Se-Mn Se und Zn Te-MnTe. Z. Anorg. Allg. Chem. **285**, 61–69 (1956)
46. J. Tauc, R. Grigorovici, A. Vancu, Optical properties and electronic structure of amorphous germanium. Physica Status Solidi (b) **15**, 627–637 (1966)
47. A. Karimi, B. Sohrabi, M.R. Vaezi, Highly transparent, flexible and hydrophilic ZnS thin films prepared by a facile and environmentally friendly chemical bath deposition method. Thin Solid Films **651**, 97–110 (2018)
48. B. Belache, Y. Khelfaoui, M. Bououdina, T. Souier, W. Cai, Structural and optical properties of silica single-layer films doped with ZnS quantum dots: photoluminescence monitoring of annealing-induced defects. Mater. Sci. Semicond. Process. **76**, 42–49 (2018)
49. Y.-T. Nien, I.-G. Chen, Raman scattering and electroluminescence of ZnS: Cu, Cl phosphor powder. Appl. Phys. Lett. **89**, 261906 (2006)
50. S.R. Chalana, V.P. Mahadevan-Pillai, Substrate dependent hierarchical structures of RF sputtered ZnS films. Appl. Surf. Sci. **440**, 1181–1195 (2018)
51. J. Trajić, R. Kostić, N. Romčević, M. Romčević, M. Mitrić, V. Lazović, P. Balaž, D. Stojanović, Raman spectroscopy of ZnS quantum dots. J. Alloys Compd. **637**, 401–406 (2015)
52. V. Senay, S. Ozen, S. Pat, S. Korkmaz, A study on some physical properties of a Pb-doped GaAs thin film produced by thermionic vacuum arc. J. Alloys Compd. **720**, 383–387 (2017)